Original Article

Institution of MECHANICAL ENGINEERS

Journal of MATERIALS: DESIGN AND APPLICATIONS

Proc IMechE Part L:
J Materials: Design and Applications
2015, Vol. 229(6) 481–492

DOI: 10.1177/1464420714532792
pil.sagepub.com
SAGE

Estimation of loss factors of a constrained layer plate using viscoelastic layer

K Kishore Kumar[1], Y Krishna[1] and P Bangarubabu[2]

Abstract

A finite element method is developed and validated for the estimation of loss factors of a viscoelastically damped plate. Viscoelastic layer is used as constrained layer and is sandwiched between an aluminum base plate and a constraining layer. Frequency-dependent material properties are used for the viscoelastic material in the finite element model. The derived dynamic equations of motion are used to carry out harmonic analysis to determine the natural frequencies and loss factors of sandwich plate and validated with experimental results for cantilever boundary condition. The validated finite element model is then used to estimate the loss factors of sandwich plate with various boundary conditions and different thicknesses of constraining and constrained layer for a given base plate thickness. The results show that the loss factor is maximum for a constraining layer to sandwich plate thickness ratio of 0.40–0.45 and is independent of boundary condition. The loss factor increases with increase in thickness of the viscoelastic layer. The loss factor increases for higher mode for all boundary conditions.

Keywords

Loss factor, viscoelastic layer, sandwich plate, frequency response function, finite element method

Date received: 20 November 2013; accepted: 25 March 2014

Introduction

Viscoelastic materials (VEM) are being widely used in aerospace structures to suppress vibrations. One of the effective methods of using VEM to damp out the vibration is in the form of constrained layer, popularly known in the literature as constrained layer damping (CLD). Energy absorbing polymer (EAP) is the VEM used in the present work. In CLD, viscoelastic layer is glued between base and constraining layer plate. Flexural vibrations of constrained layer cause shearing strain in the viscoelastic layer which dissipates energy and thereby reduce vibrations. The growing use of such structures has motivated many researchers to study sandwich structures. Adding viscoelastic layer to a structure and predicting the response is a challenging task. This is because of the EAP which is viscoelastic in nature and has frequency- and temperature-dependent material properties.

The fundamental work in this field was pioneered by Ross et al.[1] who used a three layer model to predict damping in plates with CLD treatment. They studied simply supported plates and assumed a perfect interface and compatibility of transverse displacement in each layer. Kerwin[2] presented an analysis for a simply supported sandwich beam using complex modulus to account for damping and stiffness of viscoelastic core. He observed that the energy dissipation mechanism in the constrained core is due to its shear motion. Several researchers like DiTaranto,[3] Mead and Markus,[4] Mead,[5] and Rao[6] extended Kerwin's work. Nakra[7–9] has carried out an exhaustive literature review on the topic, dealing with vibration control with VEMs. Modeling of sandwich beams is discussed by Barbosa and Farage[10] and Amichi and Atalla.[11]

The three-layered plate, with highly damped viscoelastic central layer has high damping capacity and high resistance to resonant vibrations. Ha[12] has given overview of finite element analysis of sandwich plate. The damping properties of fiber reinforced plastic laminated plate have been improved by adding relatively thin highly damped VEM between the laminated faces. This type of plate has been investigated by Cupial and Niziol[13] and Richards et al.[14] They used Reissner–Mindlin plate theory and assumed complex modulus as constant over a frequency range. Wang et al.[15] have used frequency-dependent complex shear modulus using Golla–Hughes–McTavish method.

[1]Defence Research and Development Laboratory, Hyderabad, India
[2]Department of Mechanical Engineering, National Institute of Technology, Warangal, India

Corresponding author:
K Kishore Kumar, Defence Research and Development Laboratory, Hyderabad 500 058, India.
Email: kalahasti_kishorekumar@yahoo.com

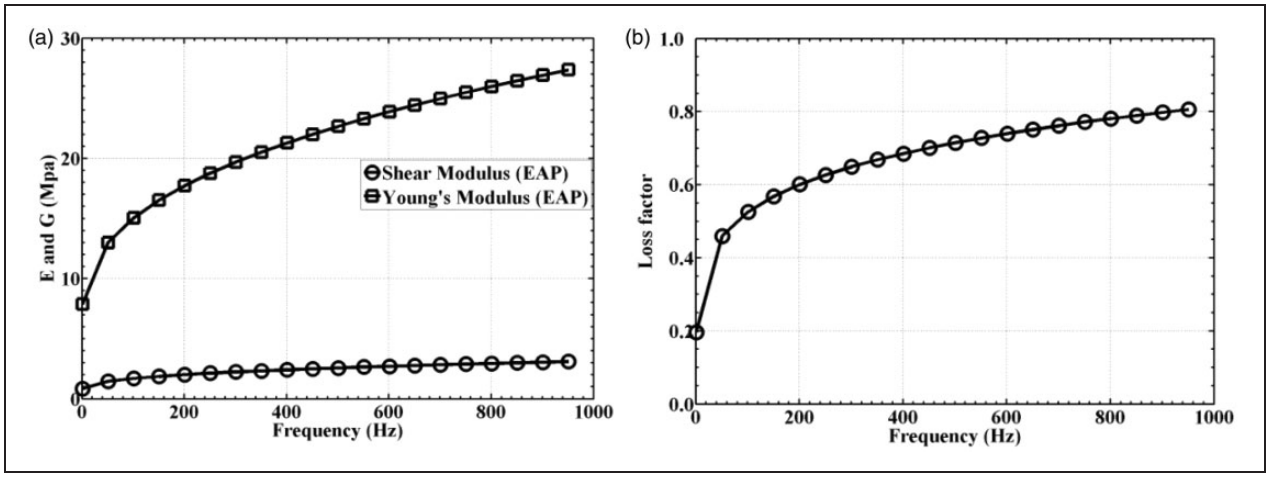

Figure 1. (a) Variation of Young's and shear modulus of EAP with frequency. (b) Variation of loss factor of EAP with frequency.

Torvik and Runyon[16] studied the loss factor of plates with CLD treatment for various boundary conditions and considered shear modulus and loss factor as constant over a frequency range. Matinez and Elejabarrieta[17,18] have carried out characterization and modeling of viscoelastic damped structures.

The present paper discusses the modeling of the sandwich plate using Reissner–Mindlin plate theory considering the frequency-dependent complex modulus and loss factors of EAP for predicting frequency response function (FRF) of the sandwich plate. Complex moduli of viscoelastic layer at discrete frequencies are obtained from the dynamic mechanical analyzer (DMA). Experiments are conducted in clamped (C) at one edge and free (F) at other three edges (CFFF) boundary condition to validate the FE model. The validated finite element (FE) model of sandwich plate is used to evaluate the loss factors for different ratios of constraining layer to sandwich plate thicknesses (t_c/t) and constrained layer to sandwich plate thicknesses (t_v/t) for various boundary conditions.

Frequency-dependent properties of VEM

The VEM is evaluated for its Young's Modulus, shear modulus, and loss factor in the DMA. The VEM is a blend of nitrile-butadiene rubber and polyvinyl chloride. The filler material is reinforcing carbon black. Figure 2 shows the variation of Young's modulus, shear modulus, and loss factors with frequency for a reference temperature of 25 °C. The strain amplitude is maintained at 0.5%. The glass transition temperature of EAP is −5 °C. The shear modulus, Young's modulus, and loss factors that are obtained from DMA are used to calculate complex shear and Young's modulus as given below

$$G^*(f) = G^v(f)(1 + i\eta'(f)) \quad (1)$$

$$E^*(f) = E^v(f)(1 + i\eta'(f)) \quad (2)$$

where $\eta'(f)$ is the frequency-dependent loss factor of the VEM. The shear modulus $G^v(f)$ and Young's modulus $E^v(f)$ for EAP can be represented by

$$G^v(f) = a_{12}f^{b_{22}} + c_{12} \quad (3)$$

$$E^v(f) = a_{11}f^{b_{11}} + c_{11} \quad (4)$$

and loss factor $\eta'(f)$ can be represented as

$$\eta'(f) = a_{13}f^{b_{13}} + c_{13} \quad (5)$$

where the constants a_{11}, b_{11}, c_{11}, a_{12}, b_{12}, c_{12}, a_{13}, b_{13}, and c_{13} are obtained from the curve fit of measured data. The variation of Young's modulus, shear modulus, and loss factors with frequency is shown in Figure 1(a) and (b), respectively. The curve-fit values are presented in Table 1.

Modeling of sandwich plate

Mathematical formulation

The equations of sandwich plate are developed based on the following assumptions: (a) The in-plane stresses in the viscoelastic (constrained) layer are much smaller than the in-plane stresses in the base or constraining layer and so may be neglected. (b) The transverse displacement w(x,y,t) is assumed to be same for all layers. (c) Linear theories of elasticity and viscoelasticity are used. (d) There is no slip at the interfaces between the viscoelastic and base plate and viscoelastic and constrained layer.

The three-layered plate under consideration and the layer displacements are shown in Figure 2. In this figure, u_1 and u_3 represent the mid-plane displacement of the base plate and the constraining layer along x-axis, respectively; α_1 and α_3 are the rotations of the normals to the mid-planes of the base plate and the constraining layer, respectively; and α_2 is the rotation of the normal to the mid-plane of the viscoelastic

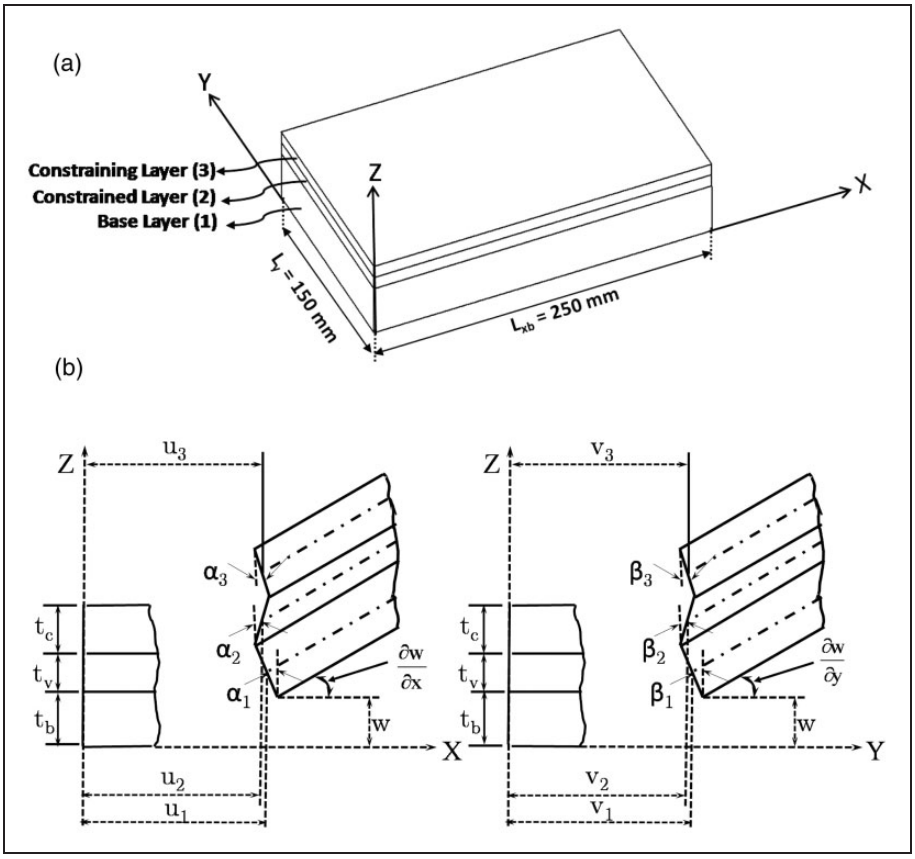

Figure 2. (a) Co-ordinates and dimensions, (b) displacements associated with each layer of sandwich plate.

Table 1. Constants of EAP obtained from curve fit of DMA data.

Property	Constants		
Young's modulus, E^v	$a_{11} = 1.599 \times 10^6$	$b_{11} = 0.3933$	$c_{11} = -9.86 \times 10^5$
Shear modulus, G^v	$a_{12} = 0.1807 \times 10^6$	$b_{12} = 0.3869$	$c_{12} = 0.2789 \times 10^6$
Loss factor, η'	$a_{13} = 0.4012$	$b_{13} = 0.174$	$c_{13} = -0.0679$

core. A similar deformation pattern is considered in the y-direction as well.

With the shear deformation accounted for the three layers, the displacements in each layer are given by[13]

$$\hat{u}_i(x, y, z, t) = u_i(x, y, t) + z\alpha_i(x, y, t) \quad (6)$$

$$\hat{v}_i(x, y, z, t) = v_i(x, y, t) + z\beta_i(x, y, t) \quad (7)$$

$$\hat{w}_i(x, y, z, t) = w(x, y, t) \quad (8)$$

where $i = 1$ for base plate, $i = 2$ for constrained layer, and $i = 3$ for constraining layer.

The z co-ordinate is measured from the mid-plane of the each layer. With above displacements, the strain in *i*th layer can be written in terms of displacements as follows

$$\epsilon_x^i = \epsilon_{ox}^i + zk_x^i, \quad \epsilon_y^i = \epsilon_{oy}^i + zk_y^i, \quad \epsilon_z = 0$$
$$\gamma_{xy}^i = \gamma_{oxy}^i + zk_{xy}^i, \quad \gamma_{xz}^i = \alpha_i + \frac{\partial w}{\partial x}, \quad \gamma_{yz}^i = \beta_i + \frac{\partial w}{\partial y} \quad (9)$$

Where, the mid-plane strains and the curvatures appearing in the above equations are represented in terms of displacements as

$$\epsilon_{ox}^i = \frac{\partial u_i}{\partial x}, \quad \epsilon_{oy}^i = \frac{\partial v_i}{\partial y}, \quad \gamma_{oxy}^i = \frac{\partial u_i}{\partial y} + \frac{\partial v_i}{\partial x}$$
$$k_x^i = \frac{\partial \alpha_i}{\partial x}, \quad k_y^i = \frac{\partial \beta_i}{\partial y}, \quad k_{xy}^i = \frac{\partial \alpha_i}{\partial y} + \frac{\partial \beta_i}{\partial x} \quad (10)$$

The continuity of displacements at the interfaces between the core and the base plate and constraining layers requires that the following relation hold

$$u_1 + \frac{t_b}{2}\alpha_1 = u_2 - \frac{t_v}{2}\alpha_2; \quad u_2 + \frac{t_v}{2}\alpha_2 = u_3 - \frac{t_c}{2}\alpha_3 \quad (11)$$

Similar equations are obtained in y-direction, by replacing u_i with v_i and α_i with β_i. From these equations the in-plane displacements and rotations of the

viscoelastic core can be expressed in terms of the in-plane displacements and rotations of the face layers

$$\begin{aligned} u_2 &= \frac{1}{2}(u_1+u_3)+\frac{1}{4}(t_b\alpha_1 - t_c\alpha_3) \\ v_2 &= \frac{1}{2}(v_1+v_3)+\frac{1}{4}(t_b\beta_1 - t_c\beta_3) \end{aligned} \tag{12}$$

$$\begin{aligned} \alpha_2 &= \frac{1}{t_v}(u_3-u_1)-\frac{1}{2t_v}(t_b\alpha_1 + t_c\alpha_3) \\ \beta_2 &= \frac{1}{t_v}(v_3-v_1)-\frac{1}{2t_v}\left(t_b\beta_1 + t_c\beta_3\right) \end{aligned} \tag{13}$$

FE model of sandwich plate

The sandwich plate is modeled using Reissner–Mindlin plate theory to evaluate the dynamic properties. The plate is discretized using four noded plate element, with nine degrees of freedom (DOF) at each node. Finite element code is developed in MATLAB®. The plate is discretized into elements along the x-direction and y-direction. The element stiffness and mass matrices are obtained as given in the following subsections.

Element stiffness matrix of sandwich plate

The complex stiffness matrix $[K^*]_k$ of the kth element of the sandwich plate is given by

$$\begin{aligned} [K^*]_k = &\left[K_{cp}\right]_k + [K_{cb}]_k + [K_{cs}]_k + \left[K^*_{sv}\right]_k \\ &+ \left[K_{bp}\right]_k + [K_{bb}]_k + [K_{bs}]_k \end{aligned} \tag{14}$$

where $[K_{cp}]$, $[K_{cb}]$, $[K_{cs}]$ are the in-plane, bending, and shear stiffness of the constraining layer; $\left[K^*_{sv}\right]$ is the shear stiffness of viscoelastic layer; and $[K_{bp}]$, $[K_{bb}]$, $[K_{bs}]$ are the in-plane, bending, and shear stiffness of the base layer. The size of element stiffness matrix is 36×36.

These stiffness matrices are given by

$$\left[K_{cp}\right]_k = |J| \int_{-1}^{1}\int_{-1}^{1} \left[B_{cp}\right]^T \left[D_{3p}\right]\left[B_{cp}\right] d\xi d\eta \tag{15}$$

$$[K_{cb}]_k = |J| \int_{-1}^{1}\int_{-1}^{1} [B_{cb}]^T [D_{3b}][B_{cb}] d\xi d\eta \tag{16}$$

$$[K_{cs}]_k = |J| \int_{-1}^{1}\int_{-1}^{1} [B_{cs}]^T [D_{3s}][B_{cs}] d\xi d\eta \tag{17}$$

$$\left[K^*_{sv}\right]_k = |J| \int_{-1}^{1}\int_{-1}^{1} [B_{sv}]^T [D_{sv}][B_{sv}] d\xi d\eta \tag{18}$$

$$\left[K_{bp}\right]_k = |J| \int_{-1}^{1}\int_{-1}^{1} \left[B_{bp}\right]^T \left[D_{1p}\right]\left[B_{bp}\right] d\xi d\eta \tag{19}$$

$$[K_{bb}]_k = |J| \int_{-1}^{1}\int_{-1}^{1} [B_{bb}]^T [D_{1b}][B_{bb}] d\xi d\eta \tag{20}$$

$$[K_{bs}]_k = |J| \int_{-1}^{1}\int_{-1}^{1} [B_{bs}]^T [D_{1s}][B_{bs}] d\xi d\eta \tag{21}$$

where

$$\left[B_{cp}\right] = \begin{bmatrix} \{N_3\}_{,x} \\ \{N_4\}_{,y} \\ \{N_3\}_{,y} + \{N_4\}_{,x} \end{bmatrix} \tag{22}$$

$$[B_{cb}] = [B_{bb}] = \begin{bmatrix} \{N_5\}_{,xx} \\ \{N_5\}_{,yy} \\ 2\{N_5\}_{,xy} \end{bmatrix} \tag{23}$$

$$[B_{cs}] = \begin{bmatrix} \{N_8\} + \dfrac{\partial w}{\partial x} \\ \{N_9\} + \dfrac{\partial w}{\partial y} \end{bmatrix} \tag{24}$$

$$[B_{sv}] = \begin{bmatrix} \left[\left(\{N_3\}-\{N_1\}\right)/t_v - \left(\left(t_b\{N_6\}+t_c\{N_8\}\right)/2t_v\right)\right] + \{N_5\}_{,x} \\ \left[\left(\{N_4\}-\{N_2\}\right)/t_v - \left(\left(t_b\{N_7\}+t_c\{N_9\}\right)/2t_v\right)\right] + \{N_5\}_{,y} \end{bmatrix} \tag{25}$$

$$\left[B_{bp}\right] = \begin{bmatrix} \{N_1\}_{,x} \\ \{N_2\}_{,y} \\ \{N_1\}_{,y} + \{N_2\}_{,x} \end{bmatrix} \tag{26}$$

$$[B_{bs}] = \begin{bmatrix} \{N_6\} + \dfrac{\partial w}{\partial x} \\ \{N_7\} + \dfrac{\partial w}{\partial y} \end{bmatrix} \tag{27}$$

$$\left[D_{ip}\right] = \frac{E_i t_i}{\left(1-v_i^2\right)} \begin{bmatrix} 1 & v_i & 0 \\ \upsilon_i & 1 & 0 \\ 0 & 0 & (1-\upsilon_i)/2 \end{bmatrix} \tag{28}$$

$$[D_{ib}] = \frac{E_i t_i^3}{12\left(1-v_i^2\right)} \begin{bmatrix} 1 & v_i & 0 \\ \upsilon_i & 1 & 0 \\ 0 & 0 & (1-\upsilon_i)/2 \end{bmatrix} \tag{29}$$

$$[D_{is}] = G_i t_i \begin{bmatrix} 1 & 0 \\ 0 & 1 \end{bmatrix} \tag{30}$$

$i=1$ for base layer (t_b) and $i=3$ for constraining layer (t_c)

$$[D_{sv}] = G^* t_v \begin{bmatrix} 1 & 0 \\ 0 & 1 \end{bmatrix} \text{ where } G^* \text{ is the frequency} - \text{dependent complex shear modulus} \tag{31}$$

$$[J] = \begin{bmatrix} \frac{\partial x}{\partial \xi} & \frac{\partial y}{\partial \xi} \\ \frac{\partial x}{\partial \eta} & \frac{\partial y}{\partial \eta} \end{bmatrix} \tag{32}$$

Element mass matrix of sandwich plate

The mass matrix for the kth element of the sandwich plate is given by

$$[M]_k = [M_b]_k + [M_{bp}]_k + [M_{cp}]_k + [M_{br}]_k + [M_{cr}]_k + [M_{vp}]_k + [M_{vr}]_k \tag{33}$$

where $[M_b]_k$ denotes the mass matrix due to bending and $[M_{bp}]_k$, $[M_{cp}]_k$, and $[M_{vp}]_k$ denote mass matrices due to extension for base layer, constraining layer, and viscoelastic layer, respectively. $[M_{br}]_k$, $[M_{cr}]_k$, and $[M_{vr}]_k$ denote matrices due to rotary inertia for base layer, constraining layer, and viscoelastic layer, respectively. These matrices are given by

$$[M_b]_k = (\rho_1 t_b + \rho_2 t_v + \rho_3 t_c)|J| \int_{-1}^{1}\int_{-1}^{1} \{N_5\}^T\{N_5\} d\xi d\eta \tag{34}$$

$$[M_{bp}]_k = \rho_1 t_b |J| \int_{-1}^{1}\int_{-1}^{1} \left(\{N_1\}^T\{N_1\} + \{N_2\}^T\{N_2\}\right) d\xi d\eta \tag{35}$$

$$[M_{cp}]_k = \rho_3 t_c |J| \int_{-1}^{1}\int_{-1}^{1} \left(\{N_3\}^T\{N_3\} + \{N_4\}^T\{N_4\}\right) d\xi d\eta \tag{36}$$

$$[M_{br}]_k = \frac{\rho_1 t_b^3}{12} |J| \int_{-1}^{1}\int_{-1}^{1} \left(\{N_6\}^T\{N_6\} + \{N_7\}^T\{N_7\}\right) d\xi d\eta \tag{37}$$

$$[M_{cr}]_k = \frac{\rho_3 t_c^3}{12} |J| \int_{-1}^{1}\int_{-1}^{1} \left(\{N_8\}^T\{N_8\} + \{N_9\}^T\{N_9\}\right) d\xi d\eta \tag{38}$$

$$[M_{vp}]_k = \rho_2 t_v \int_A \{N\}^T[C_v]\{N\} dA \tag{39}$$

$$[M_{vr}]_k = \frac{\rho_2 t_v^3}{12} \int_A \{N\}^T[D_v]\{N\} dA \tag{40}$$

The size of the element mass matrix is 36×36.

Equations of motion

The equation of motion of sandwich plate subjected to base excitation[19] can be written as

$$[M]\{\ddot{w}(t)\} + [K^*]\{w(t)\} = 0 \tag{41}$$

where $[K^*]$ is the frequency-dependent global complex stiffness matrix that varies with frequency-dependent shear modulus (G) and loss factor (η) as given in equations (3) and (5), $\{w\}$ is the transverse displacement vector, and [M] is the global mass matrix and can be written as

$$[M]\{\ddot{w}(t)\} + [K(1+i]\{w(t)\} = 0 \tag{42}$$

For base excitation problem, equation (42) can be written as

$$\begin{bmatrix} M_{cc} & M_{cu} \\ M_{uc} & M_{uu} \end{bmatrix} \begin{Bmatrix} \ddot{w}_c(t) \\ \ddot{w}_u(t) \end{Bmatrix} + \begin{bmatrix} K^*_{cc} & K^*_{cu} \\ K^*_{uc} & K^*_{uu} \end{bmatrix} \begin{Bmatrix} w_c(t) \\ w_u(t) \end{Bmatrix} = \begin{Bmatrix} 0 \\ 0 \end{Bmatrix} \tag{43}$$

where $w(x,t) = \{w_c(x,t)\ w_u(x,t)\}$, where $w_c(x,t)$ is the constrained DOF and $w_u(x,t)$ is the unconstrained DOF. The subscript cc and uu represent constrained and unconstrained part of mass and complex stiffness matrices. Equation (41) can be written as

$$\begin{bmatrix} M_{cc} & M_{cu} \\ M_{uc} & M_{uu} \end{bmatrix} \begin{Bmatrix} \ddot{w}_c \\ \psi \ddot{w}_c + w_d \end{Bmatrix} + \begin{bmatrix} K^*_{cc} & K^*_{cu} \\ K^*_{uc} & K^*_{uu} \end{bmatrix} \text{times} \begin{Bmatrix} w_c \\ \psi w_c + w_d \end{Bmatrix} = \begin{Bmatrix} 0 \\ 0 \end{Bmatrix} \tag{44}$$

where $[\psi] = \left[K^*_{uu}\right]^{-1}[K^*_{uc}]$ is constant and dimensionless.

Applying the constraints and ignoring off diagonal terms, equation (44) reduces to

$$[M_{uu}]\{\ddot{w}_d\} + \left[K^*_{uu}\right]\{w_d\} = -\{[\psi][M_{uu}] + [M_{uc}]\}\{\ddot{w}_c\} \tag{45}$$

For harmonic base acceleration input$\{\ddot{w}_c\}$, equation (45) is solved for the response and FRFs are constructed. In evaluating complex global stiffness matrix of sandwich plate, the loss factor of the viscoelastic layer is obtained from DMA tests and for base plate is obtained from modal testing.

Experimental setup

An aluminum base plate is constrained at one edge and free at other three edges (CFFF) to understand the loss factors of the first three modes. To study the enhancement of loss factors, VEM is glued between the base and constraining layer. The constraining layer is also made of aluminum plate. The dimensions and material properties of base plate, constrained (EAP), and constraining layer used for experiment and FE studied are given in Table 2. Experiments are conducted with two thicknesses of t_c/t equals to 0.16 and 0.18 and t_v/t equals to 0.09 and 0.17 for validation of FE model. The constrained and

Table 2. Material and dimensions of sandwich plate.

Sandwich plate	Length (mm)	Width (mm)	Thickness (mm)	Material properties	
				Density (ρ), kg/m^3	Young's modulus (MPa) Shear modulus (MPa)
Base plate (1)	$L_{xb} = 250$	Ly = 150	$t_b = 4.00$	2740	E = 68,900 G = 23,300
Constrained layer (2)	$L_{xv} = 240$	Ly = 150	$t_v = 0.50$ and 1.00	1260	refer equations (3) and (4)
Constraining layer (3)	$L_{xc} = 240$	Ly = 150	$t_c = 1.00$	2740	E = 68,900 G = 23,300

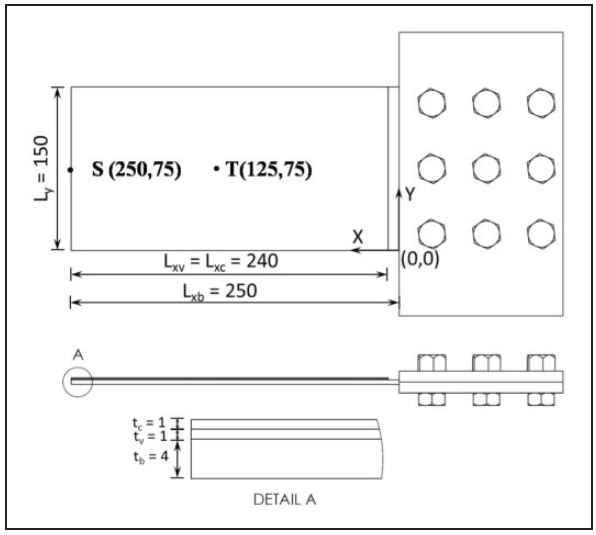

Figure 3. Schematic of constrained layer plate.

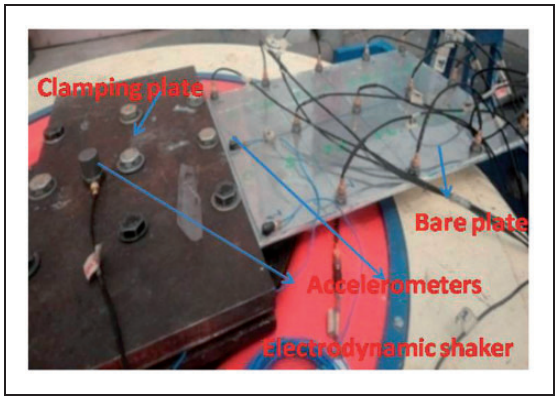

Figure 4. Photograph of experimental setup showing bare plate.

constraining layers are free at all the four edges as shown in Figure 3. Epoxy-based adhesive is used to bond the viscoelastic layer to the base and the constraining layer. A snapshot of the experimental setup is shown in Figure 4. The clamped end is in turn connected to electrodynamic shaker that gives the base excitation. Base excitation is chosen in the

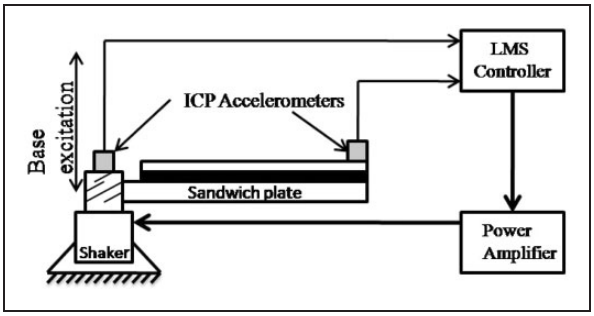

Figure 5. Schematic of test setup for acquiring FRF.

experiments to minimize the contributing of armature dynamics during evaluation of natural frequencies and loss factors of base plate and sandwich plate. An accelerometer kept on the clamped plate measures the base acceleration and the other accelerometers on the sandwich plate measure the responses. PC-based Leuven Measurement System (LMS) controller is used to provide harmonic acceleration input to the shaker. The base plate and sandwich plate are tested for a frequency band of 20–1000 Hz with a sweep rate of 1 Hz at off resonance and 0.01 Hz around resonance. The time domain base acceleration input and responses at different location of the plate are transformed to frequency domain using fast Fourier transform. The FRF is obtained from the response at a given location of plate with respect to base acceleration input. Figure 5 shows the schematic of test setup for acquiring FRF.

Results and discussion

The dimensions of sandwich plate used in FE and experiment are presented in Table 2. The sandwich plate is discretized into 25 elements along x-direction and three elements along y-direction as shown in Figure 6. The constrained and constraining layer length is 240 mm compared to base plate length of 250 mm. So, in FE model of sandwich plate, the material properties like shear modulus and density of constrained and constraining layer are degraded to a low value for the elements corresponding to 1, 26, and 51 (refer Figure 6) along the constrained edge

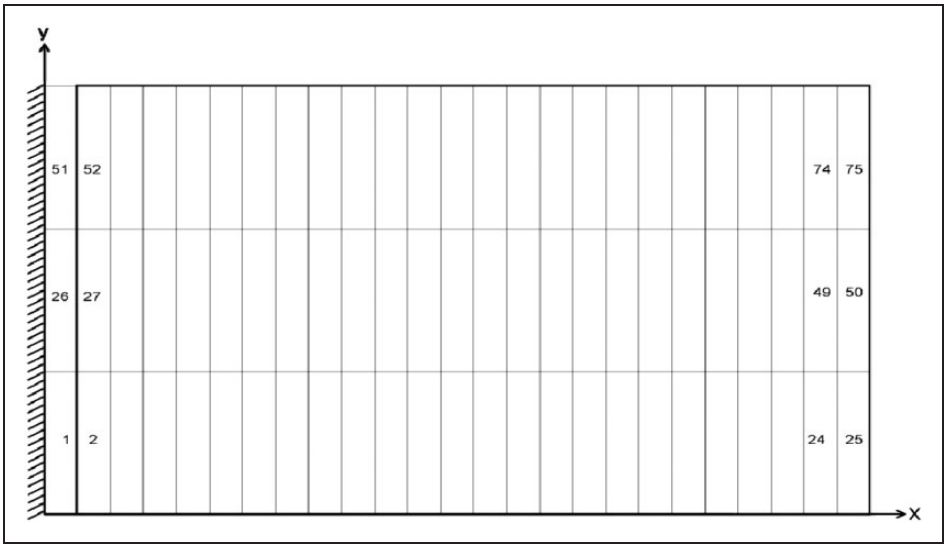

Figure 6. FE mesh of sandwich plate.

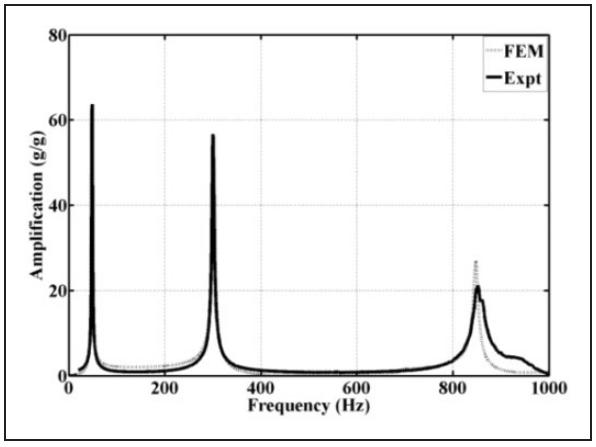

Figure 7. The FRF of base plate at point S (250, 75 mm, refer Figure 3).

so that the experimental conditions are simulated. The Young's modulus, shear modulus, and loss factor of constrained layer are frequency dependent. So, the complex stiffness is also frequency dependent. All DOFs corresponding to clamped edges are constrained. Base harmonic acceleration is applied along the constrained edge of the sandwich plate and responses are measured for various excitation frequencies from 20 to 1000 Hz. The FRF is constructed at a given location. Experiments are conducted in CFFF boundary condition for two thickness ratios of t_c/t equals to 0.16 and 0.18 and t_v/t equals to 0.09 and 0.17 for validation of FE model.

Base plate

The experimentally obtained FRF at the free end of the bare plate (Point S: 250 mm, 75 mm, see Figure 3) is compared with FE results and is shown in Figure 7 and given in Table 3. It is seen that the experimental and FE results match very well. The experimental loss factors calculated using half power method[20] for the first three modes are also given in Table 3. The damping present in the base plate is mainly due to its structural damping.

Table 3. Comparison of FEM and experimental frequencies of base plate.

	Natural frequency (Hz)		Amplification (g/g)		
Mode	FEM	Expt	FEM	Expt	Loss factor (experiment)
1	47.7	48.7	63.4	63.7	0.0152
2	301.3	302.3	54.5	56.6	0.0196
3	847.4	852.3	25.1	21.1	0.0240

FEM: finite element method.

Constrained layer sandwich plate

The FRFs of constrained layer sandwich plate at location S (250, 75 mm) and T (125, 75 mm) for two thicknesses of t_c/t equals to 0.16 and 0.18 and t_v/t equals to 0.09 and 0.17 are shown in Figures 8 and 9, respectively. It is seen that the FRF obtained from FE and experiments match very well. Tables 4 and 5 present the comparison of natural frequencies, amplification factors, and composite loss factors obtained from FE and experiments. Table 6 presents the comparison of amplification factors for base plate and sandwich plate of t_c/t of 0.16 and 0.18 and t_v/t of 0.09 and 0.17. From the table it is seen that higher attenuation is observed for higher modes. For a given mode, higher attenuation is obtained for higher thicknesses of viscoelastic layer.

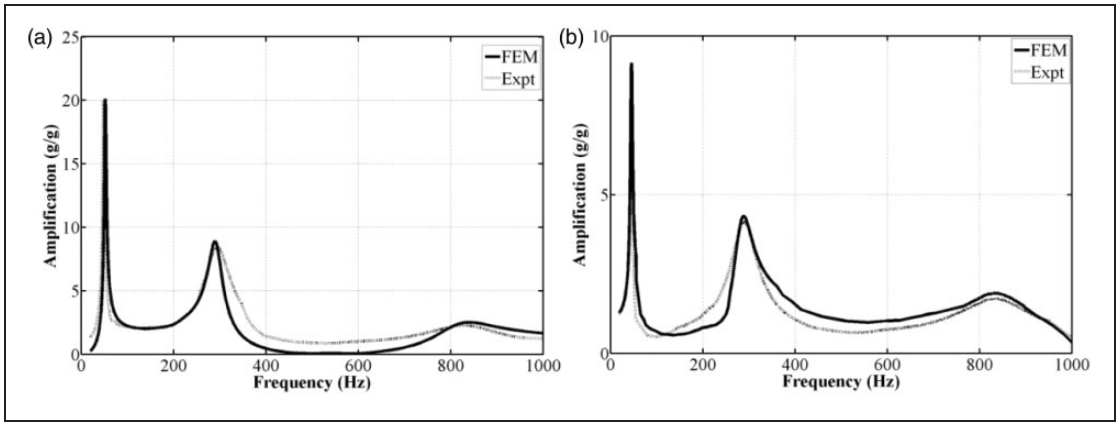

Figure 8. FRF of constrained layer plate for $t_c/t = 0.18$ and $t_v/t = 0.09$ at a point (a). S (250, 75 mm), (b) T (125, 75 mm).

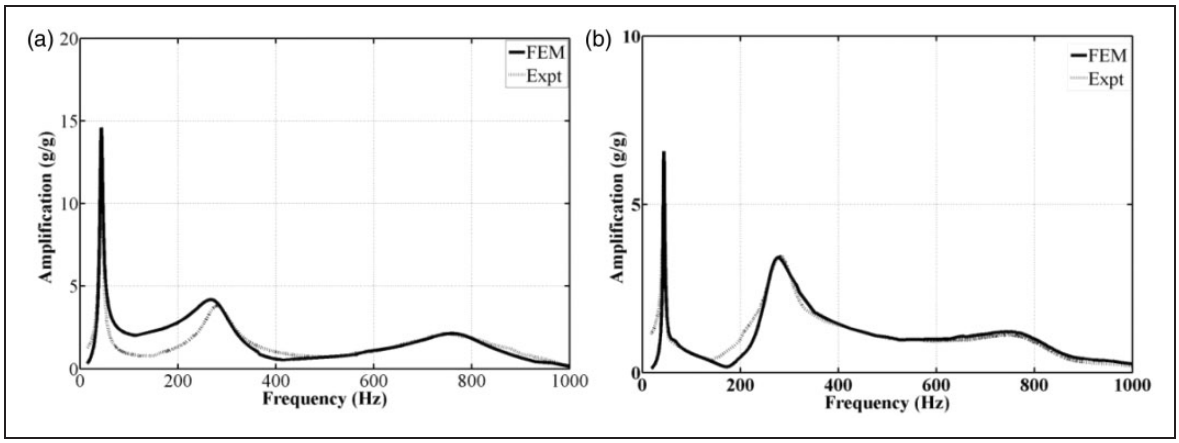

Figure 9. FRF of constrained layer plate for $t_c/t = 0.16$ and $t_v/t = 0.17$ at a point (a). S (250, 75 mm), (b) T (125, 75 mm).

Table 4. Comparison of FEM and experimental loss factors of constrained layer plate ($t_c/t = 0.18$ and $t_v/t = 0.09$).

	FEM			Expt		
Mode	Freq (Hz)	Amplification (g/g)	Loss factor	Freq (Hz)	Amplification (g/g)	Loss factor
1	45.5	19.81	0.030	45.0	18.60	0.031
2	286	8.80	0.057	281.0	8.48	0.058
3	814.0	2.50	0.070	808.0	2.30	0.073

FEM: finite element method.

Table 5. Comparison of FEM and experimental loss factors of constrained layer plate ($t_c/t = 0.16$ and $t_v/t = 0.17$).

	FEM			Expt		
Mode	Freq (Hz)	Amplification (g/g)	Loss factor	Freq (Hz)	Amplification (g/g)	Loss factor
1	43.60	14.60	0.051	43.07	14.40	0.052
2	267.20	4.20	0.080	273.8	3.80	0.083
3	759.00	2.10	0.12	740.16	1.70	0.130

Table 6. Comparison of amplification factors for bare and constrained layer plate.

Configuration/ Mode	Base plate amplification, g/g (dB)	Sandwich plate ($t_c/t = 0.18$; $t_v/t = 0.09$)amplification, g/g (dB)	Sandwich plate ($t_c/t = 0.16$; $t_v/t = 0.17$) amplification, g/g (dB)
1	63.70 (0)	18.60 (–10)	14.40 (–13)
2	56.50 (0)	8.48 (–16)	3.80 (–22)
3	21.10 (0)	2.30 (–19)	1.70 (–23)

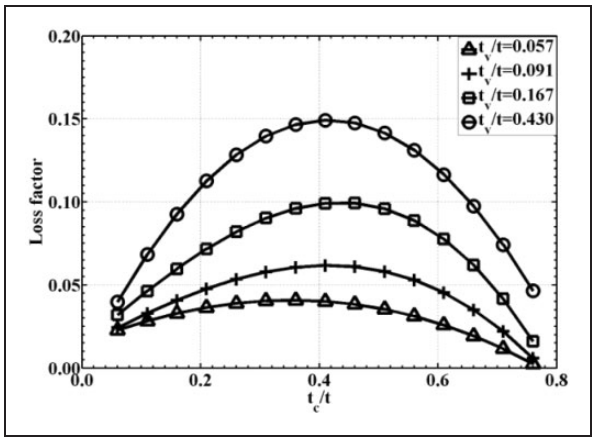

Figure 10. Variation of loss factor for CFFF boundary condition (mode I).

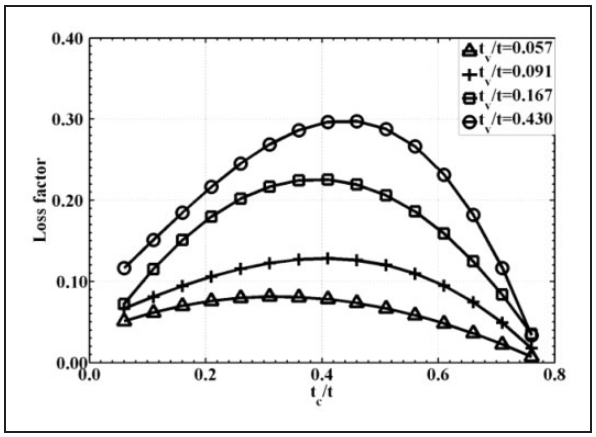

Figure 12. Variation of loss factor for CFFF boundary condition (mode III).

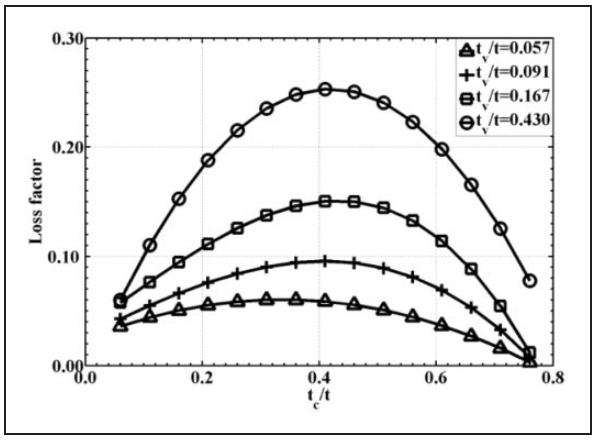

Figure 11. Variation of loss factor for CFFF boundary condition (mode II).

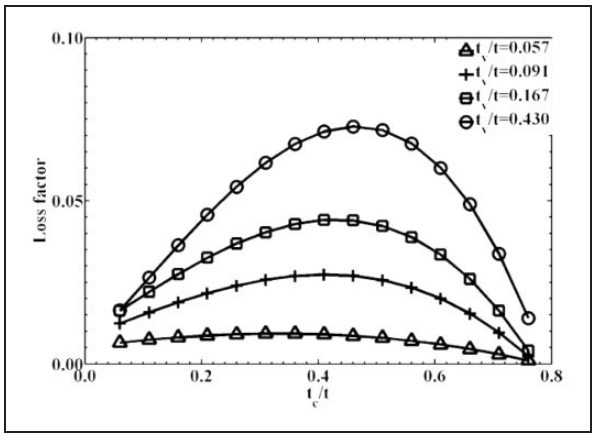

Figure 13. Variation of loss factor for SFSF boundary condition (mode I).

Numerical results of constrained layer plate (CFFF, simple support at opposite edges and free at other opposite edges (SFSF), and free at all four edges (FFFF) boundary conditions)

The validated FE model is used to compute the loss factors of constrained layer plate for various thicknesses of constraining and constrained layer in CFFF, SFSF, and FFFF boundary conditions. The variation of loss factor with the ratio of constraining layer thickness to total sandwich plate thickness (t_c/t) for first three modes in CFFF, SFSF, and FFFF boundary conditions is shown in Figures 10 to 12, 13 to 15, and 16 to 18, respectively. From Figures 10 to 18, it is observed that the loss factors are maximum when t_c/t lies between 0.4 and 0.45. The neutral axis of sandwich plate lies in constrained layer, when t_c/t lies between 0.4 and 0.45. So, the shear strain is maximum if the neutral axis of the sandwich plate falls in the constrained layer. It is also seen that

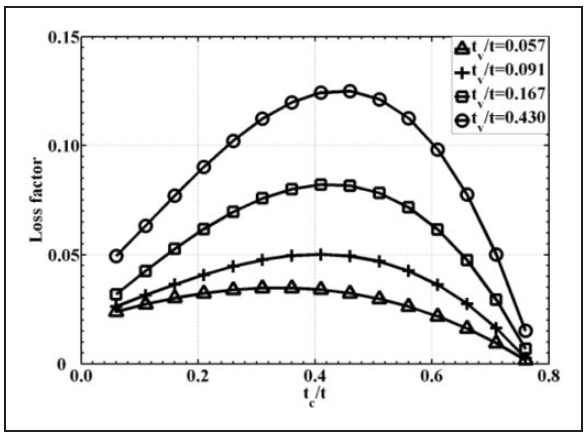

Figure 14. Variation of loss factor for SFSF boundary condition (mode II).

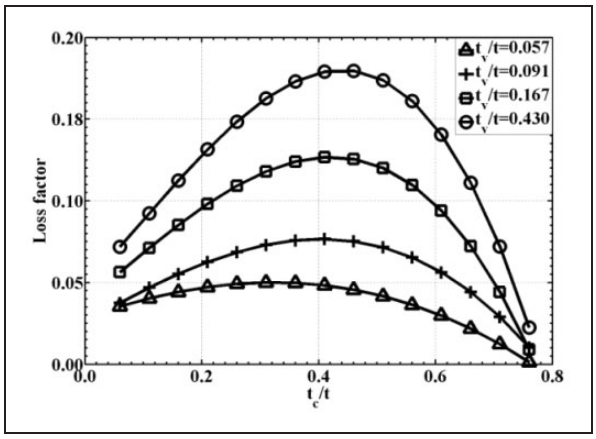

Figure 15. Variation of loss factor for SFSF boundary condition (mode III).

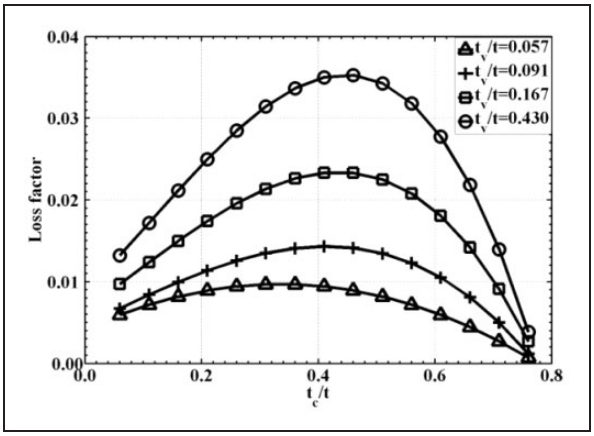

Figure 16. Variation of loss factor for FFFF boundary condition (mode I).

the peak value of loss factor is independent of boundary conditions. The loss factors increase with increase in t_v/t ratio for all modes and boundary conditions, and for a given t_v/t the loss factor is higher for higher modes for all the boundary conditions.

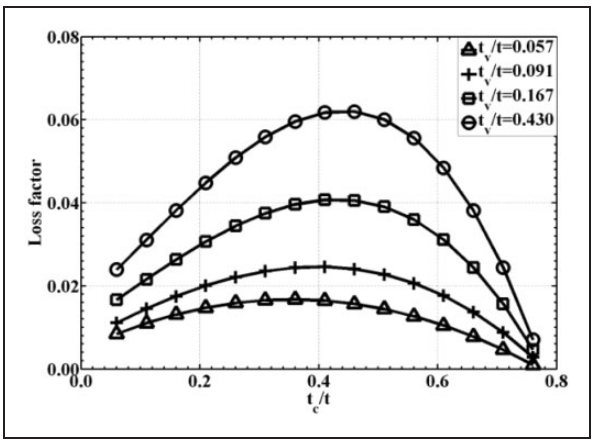

Figure 17. Variation of loss factor for FFFF boundary condition (mode II).

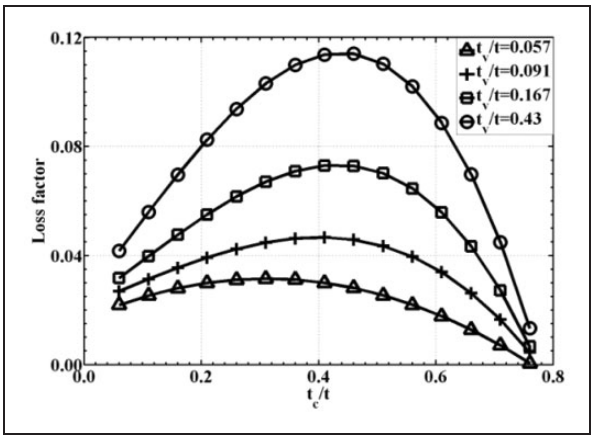

Figure 18. Variation of loss factor for FFFF boundary condition (mode III).

Applications

The use of constrained layer viscoelastic structures results in higher loss factors and this has potential applications in aerospace vehicles and automobiles. Aerospace vehicles are exposed to severe broadband vibrations due to boundary layer noise. It is essential that for proper functioning of avionics, a vibration free environment has to be ensured. This can be achieved by using viscoelastic layer sandwich structures where it is possible to obtain very high loss factors. Also, high loss factors help in suppressing the response around resonance. Depending upon the acceptable response, the design parameters of the sandwich structure can be finalized.

Conclusions

The frequency-dependent Young's modulus and loss factors expressed in power series for EAP are

introduced in the sandwich plate FE model using iterative scheme. The composite loss factors of sandwich plate using FEM compare very well with those obtained from experimental results in CFFF boundary condition for two thicknesses ratios. After the validation of FE model with experiment for CFFF boundary condition with two thickness ratios, numerical studies are carried out for CFFF, SFSF, and FFFF boundary conditions for various thickness of constraining and constrained layer. It is observed from the numerical studies that the highest loss factor is obtained when t_c/t lies between 0.4 and 0.45 for all modes and boundary conditions. This corresponds to the neutral axis of sandwich plate falls in constrained layer (viscoelastic layer) where the shear strain is maximum. The loss factor also increases for higher t_v/t ratios and it is independent of boundary conditions. The loss factor is higher for higher modes.

Acknowledgements

The authors are thankful to Director, Defence Research and Development Laboratory (DRDL), Hyderabad, India for giving permission to pursue research in the area of layer damping treatment. The authors would like to thank NMRL, Ambernath for providing viscoelastic material.

Funding

This research received no specific grant from any funding agency in the public, commercial, or not-for-profit sectors.

References

1. Ross D, Ungar EE and Kerwin EM Jr. Damping of flexural vibrations by means of viscoelastic laminae. In: JE Ruzicka (ed.) *Structural damping: Colloquium on structural damping*, Sec. III, ASME Annual Meeting, New York, 1959, pp.49–88.
2. Kerwin EM Jr. Damping of flexural waves by a constrained viscoelastic layer. *J Acoust Soc Am* 1959; 31: 952–962.
3. DiTaranto RA. Theory of vibratory bending for elastic and viscoelastic layered finite length beams. *ASME J Appl Mech* 1965; 87: 881–886.
4. Mead DJ and Markus S. The forced vibration of a three-layer damped sandwich beams with arbitrary boundary conditions. *J Sound Vib* 1969; 10: 163–175.
5. Mead DJ. Loss factors and resonant frequencies of encastre damped sandwich beams. *J Sound Vib* 1970; 12: 99–112.
6. Rao DK. Frequency and loss factors of sandwich beams under various boundary conditions. *J Mech Eng Sci* 1978; 20: 271–282.
7. Nakra BC. Vibration control with viscoelastic materials I. *Shock Vib Digest* 1976; 8: 3–12.
8. Nakra BC. Vibration control with viscoelastic materials II. *Shock Vib Digest* 1981; 13: 17–20.
9. Nakra BC. Vibration control with viscoelastic materials III. *Shock Vib Digest* 1984; 16: 17–22.
10. Barbosa FS and Farage MCR. A finite element model for sandwich viscoelastic beams: Experimental and numerical assessment. *J Sound Vib* 2008; 317: 91–111.
11. Amichi K and Atalla N. A new 3D finite element for sandwich beams with a viscoelastic core. *J Vib Acoust* 2009; 131: 3930–3943.
12. Ha KH. Finite element analysis of sandwich plates: An overview. *Comput Struct* 1990; 37: 397–403.
13. Cupial P and Niziol J. Vibration and damping analysis of a three-layered composite plate with a viscoelastic mid layer. *J Sound Vib* 1995; 183: 99–114.
14. Richards R, Chate A and Barkanov E. Finite element analysis of damping the vibrations of laminated composites. *Comput Struct* 1993; 47: 1005.
15. Wang G, Veeramani S and Wereley NM. Analysis of sandwich plates with isotropic face plates and a viscoelastic core. *J Vib Acoust* 2000; 122: 305–312.
16. Torvik PJ and Runyon BD. Estimating the loss factors of plates with constrained layer damping treatments. *AIAA J* 2007; 45: 1492–1500.
17. Martinez M and Elejabarrieta MJ. Characterization and modeling of viscoelastic damped structures. *Int J Mech Sci* 2010; 52: 1225–1233.
18. Martinez M and Elejabarrieta MJ. Dynamic characterization of high damping viscoelastic materials from vibration test data. *J Sound Vib* 2011; 330: 3930–3943.
19. Kohnke P. *Theory reference*, Release 5.6, Ansys Manual, chapter 17.
20. Torvik PJ. On estimating system damping from frequency response bandwidths. *J Sound Vib* 2011; 330: 6088–6097.

Appendix I

Notation

$E^*(f)$	frequency-dependent complex Young's modulus of viscoelastic layer
$E^v(f)$	frequency-dependent real component of Young's modulus of viscoelastic layer
$G^*(f)$	frequency-dependent complex shear modulus of viscoelastic layer
$G^v(f)$	real component of frequency-dependent shear modulus of viscoelastic layer
$i = 1$ to 3	1 for base plate, 2 for constrained layer, and 3 for constraining layer
$[K^*]$	global stiffness matrix
$[K^*]_k$	complex element stiffness matrix of sandwich plate
$[K_{bb}]_k$	element bending stiffness of base layer
$[K_{bp}]_k$	element in-plane stiffness of constrained layer
$[K_{bs}]_k$	element shear stiffness of base layer
$[K_{cb}]_k$	element bending stiffness of base layer
$[K_{cp}]_k$	element in-plane stiffness of constrained layer
$[K_{cs}]_k$	element shear stiffness of base layer
$[K^*_{sv}]_k$	complex element shear stiffness of viscoelastic layer
$[K]^I$	imaginary component of global stiffness matrix
$[K]^R$	real component of global stiffness matrix
L_{xb}, L_y	length and width of the base plate

L_{xv}, L_{xc}	length of the viscoelastic layer and constraining layer
$[M]$	global stiffness matrix
$[M]_k$	element mass matrix of sandwich plate
$[M_b]_k$	mass matrix due to bending
$\left[M_{bp}\right]_k$	mass matrix due to extension of base layer
$[M_{br}]_k$	mass matrix due to rotary inertia of base layer
$\left[M_{cp}\right]_k$	mass matrix due to extension of constraining layer
$[M_{cr}]_k$	mass matrix due to rotary inertia of constraining layer
$[M_{vp}]_k$	mass matrix due to extension of constrained layer
$[M_{vr}]_k$	mass matrix due to rotary inertia of constrained layer
t	total thickness of sandwich plate
t_b, t_v, t_c	thickness of base plate, constrained, and constraining layer
t_c/t	ratio of constraining layer thickness to total sandwich plate thickness
t_v/t_b	ratio of constrained layer thickness to base plate thickness
u_i	axial displacement of plate in x-direction
v_i	axial displacement of base plate in y-direction
w	transverse displacement of all three layers
$w, \ddot{w}$	base displacement and base acceleration, respectively
α_i	rotation normal to mid-plane in x-direction
β_i	rotation normal to mid-plane in y-direction
γ^i	shear strain in ith layer
$\mathcal{E}^i$	strain in ith layer
$\eta'(f)$	frequency-dependent loss factor
ξ and η	natural co-ordinates
ρ_1, ρ_2, ρ_3	density of base plate, constrained layer, and constraining plate, respectively